Structural elucidation of the dichloridodioxido-[(4,7-dimethyl)-1,10-phenanthroline]molybdenum(VI) ($C_{14}H_{12}Cl_2MoN_2O_2$)

John D. Bonilla,[1] Hernando Camargo,[2] and Nelson J. Castellanos [1,a)]
[1]*Laboratorio de Diseño y Reactividad de Estructuras Sólidas (Lab-DRES, 125), Departamento de Química, Facultad de Ciencias, Universidad Nacional de Colombia, Carrera 30 No. 45-03, Bogotá 11321, Colombia*
[2]*Grupo de Investigación de Materiales de Interés Geológico y Geotécnico, Servicio Geológico Colombiano SGC, Diagonal 53 No. 34-53, Bogotá, Colombia*

(Received 28 January 2024; accepted 30 June 2024)

In this work, the synthesis, characterization, and X-ray powder diffraction data for dichloridodioxido-[(4,7-dimethyl)-1,10-phenanthroline]molybdenum(VI) are reported. The crystal structure of this compound was solved from powder diffraction data using the simulated annealing method with a subsequent refinement using the Rietveld method. The dioxo-molybdenum (VI) complex $C_{14}H_{12}Cl_2MoN_2O_2$ crystallizes in a monoclinic system with space group C2/c (N° 15) with refined unit-cell parameters $a = 12.9495$ (5) Å, $b = 9.7752$ (4) Å, $c = 12.0069$ (6) Å, $\beta = 101.702$ (3) °, unit-cell volume $V = 1488.27$ (11) Å^3, and values of $Z' = 0.5$ *and* $Z = 4$. The molecules are organized into chains diagonally along the *a* and *c* axis. Parallel polyhedra are observed along these axes formed by the interactions of Mo, Cl, O, and N atoms present in the coordination sphere. The crystalline packing of this dioxo-molybdenum (VI) complex is dominated by five intermolecular hydrogen bonds, two intramolecular hydrogen bonds, and the four interactions between the centroids *(CgI···CgJ)* of the aromatic rings. An analysis of the Hirshfeld surface revealed that the greatest contributions of the attractive forces are given by *H···Cl/Cl···H, H···C/C···H, H···O/O···H,* and *H···H* interactions.

[doi:10.1017/S0885715624000393]

Keywords: 1,10-phenanthrolines disubstituted, dioxo-molybdenum (VI) complex, Rietveld refinement, X-ray diffraction of polycrystalline samples

I. INTRODUCTION

In selective oxidation processes, it is a technological challenge to use atmospheric oxygen directly under ambient conditions of pressure and temperature to replace highly polluting oxidizing agents normally used, avoiding excess reagents and reducing the formation of byproducts (Anastas and Kirchhoff, 2002; Hermans et al., 2009; Roduner et al., 2013; Hone and Kappe, 2019). The activation of molecular oxygen and more specifically the action of depositing an oxygen atom on a substrate is a process that in nature is carried out by enzymes such as oxotransferases or hydroxylases, where the molybdenum-oxygen unit (Mo = O) is present as the active center (Arzoumanian, 1998; Hille, 2002; Hille et al., 2011; Heinze, 2015).

The study of these natural systems called molybdenum-enzymes has been the source of inspiration to synthesize biomimetic structures with the dioxo-Mo unit as the active center, compounds which have been used as catalysts selectively in oxygen atoms transfer (OAT) process to substrates such as phosphines, alcohols, arylalkanes, and alkenes using different oxo-donors in solution (Martínez et al., 2016; Martinez Q et al., 2020; Kargar et al., 2021; Julião et al., 2022).

Molybdenum's ability to selectively generate oxygenated products has been explained by its natural property to incorporate oxygen atoms into its coordination sphere in high oxidation states (>4) (Dupé et al., 2015; Zwettler et al., 2019). On the other hand, it has been shown that its oxotransfer capacity can be increased by factors such as the presence of a second oxo ligand in the Mo = O unit and/or the presence of ligands with a high electronic density that can provide charge density and populate the metal center to reduce the bond order and facilitate oxygen donation (Arzoumanian et al., 1994; Kühn et al., 2006).

Different studies of OAT catalyzed by dioxo-Mo complexes have been reported using bidentate dithiocarbamates, bipyridines, Schiff bases, salen-type ligands, or combinations of these, and the results have shown their high selectivity and reactivity as homogeneous and heterogenous catalysts (Arzoumanian et al., 2006; Bakhtchadjian et al., 2011; Castellanos et al., 2012, 2013, 2021; Qin et al., 2019; Bouzari et al., 2021; Nunes et al., 2023). Oxygen atom transfer processes using dioxo-Mo complexes with phenanthroline-type ligands are less frequent in the literature although this polypyridine ligand is considered one of the main symmetric platforms to obtain transition metal complexes. Its relevance

a)Author to whom correspondence should be addressed. Electronic mail: njcastellanosm@unal.edu.co

lies in the donor capacity of nitrogen atoms, which can be modulated by the incorporation of different substituents on its periphery, influencing the catalytic activity of the metal center (Shen and Patrick Sullivan, 1995; Bencini and Lippolis, 2010; Camargo et al., 2016).

In this work, we report the synthesis of a new dioxo-molybdenum (VI) complex using the bidentate ligand 1,10-phenanthroline disubstituted with methyl groups. The results obtained by NMR, elemental analysis, and infrared spectroscopy allowed the respective molecular characterization. The structural determination of the dichloridodioxido-[(4,7-dimethyl)-1,10-phenanthroline]molybdenum(VI) compound as a biomimetic complex of molybdenum-enzymes was solved from X-ray powder diffraction (XRPD) data analysis using the simulated annealing method with a subsequent refinement using the Rietveld method. The atomic coordinates were determined using the EXPO2014 program and validated using the PLATON multipurpose software.

II. EXPERIMENTAL SECTION

4,7-dimethyl-1,10-phenanthroline was obtained from Alfa Aesar and MoO_2Cl_2 was purchased from Sigma-Aldrich and used without further purification. Commercial grade solvents were dried and deoxygenated by refluxing for at least 12 h over appropriate drying agents under argon atmosphere and were freshly distilled prior to use. IR (KBr) was recorded with a Perkin-Elmer 1720XFT. ^{1}H and ^{13}C NMR were performed with Bruker Avance 400 spectrometer. The CHN elemental analysis was performed on a Thermo Scientific Flash 2000 CHNS/O analyzer equipped with a TCD detector.

A. Synthesis of dichloridodioxido-[(4,7-dimethyl)-1,10-phenanthroline]molybdenum(VI)

0.208 g (1.0 mmol) of 4,7-dimethyl-1,10-phenanthroline ligand dissolved in acetonitrile (20 mL) was slowly added under a nitrogen atmosphere to a solution of acetonitrile (20 mL) containing 0.200 g (1.0 mmol) of MoO_2Cl_2 and the reaction mixture was stirred overnight at reflux temperature (85 °C). After that, the reaction mixture was cooled to room temperature, the solid obtained separated from the reaction medium by filtration under N_2 atmosphere, and the resulting solid was washed three times with ethyl ether (3 × 20 mL) to obtain a light pink solid. (0.310 g; $\%R = 75.9$) IR (cm^{-1}) KBr: 3089 (=CH), 2991 (CH), 1622 (C = C), 1427 (C = C), 935 (Mo = O_{asym}), 899 (Mo = O_{sym}). ^{1}H NMR (400 MHz, DMSO) δ 9.17 (d, $J = 5.1$ Hz, 2H), 8.47 (s, 2H), 8.10 (d, $J = 5.1$ Hz, 2H), 2.99 (s, 6H). Elemental analysis calculated for $C_{14}H_{12}Cl_2MoN_2O_2$ (407.93): C 41.30, H 2.97, N 6.88. Found: C 41.44, H 2.99, N 6.39 (Figure 1).

B. Powder diffraction data collection

XRPD measurement of the dichloridodioxido-[(4,7-dimethyl)-1,10-phenanthroline]molybdenum(VI) complex (Figure 2, blue line) was carried out at 298 K using an

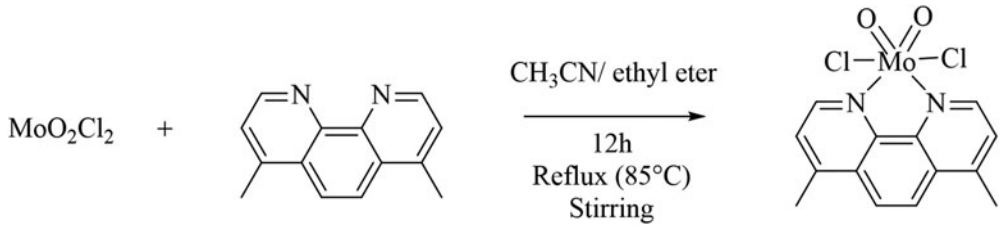

Figure 1. Synthesis of dichloridodioxido-[(4,7-dimethyl)-1,10-phenanthroline]molybdenum(VI).

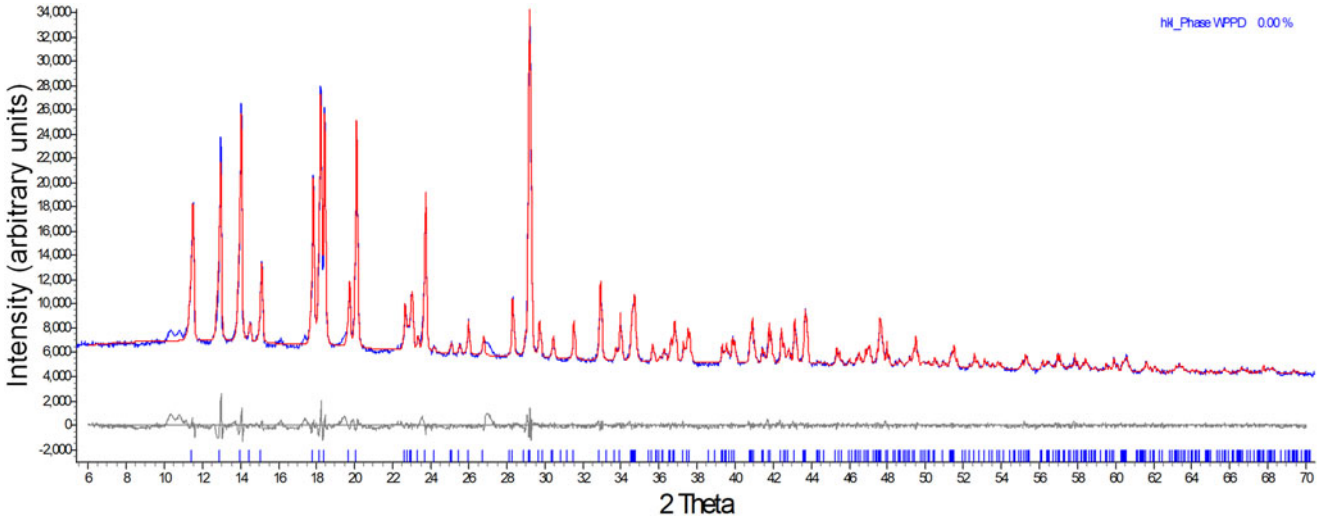

Figure 2. Experimental XRPD diffractogram of the dichloridodioxido-[(4,7-dimethyl)-1,10-phenanthroline]molybdenum(VI) using Cu Kα radiation (blue solid line) and the refined pattern obtained using WPPD procedure (red solid line).

https://doi.org/10.1017/S0885715624000393 Published online by Cambridge University Press

TABLE I. X-ray powder diffraction data obtained for the dichloridodioxido-[(4,7-dimethyl)-1,10-phenanthroline]molybdenum(VI) complex.

No.	$2\theta_{obs}$ (°)	d_{obs} (Å)	I/I_o	h	k	l	$2\theta_{cal}$ (°)	d_{cal} (Å)	$\Delta 2\theta$
1	11.472	7.7070	42	−1	1	0	11.438	7.7300	−0.034
2	12.937	6.8377	61	−1	1	1	12.904	6.8548	−0.032
3	14.011	6.3159	71	2	0	0	13.979	6.3303	−0.032
4	14.508	6.1006	7	1	1	1	14.473	6.1152	−0.035
5	15.112	5.8581	25	0	0	2	15.102	5.8617	−0.009
6	17.822	4.9729	51	−1	1	2	17.809	4.9764	−0.013
7	18.196	4.8715	77	0	2	0	18.163	4.8802	−0.033
8	18.427	4.8110	71	−2	0	2	18.413	4.8146	−0.014
9	19.713	4.5000	19	0	2	1	19.689	4.5054	−0.024
10	20.104	4.4132	66	1	1	2	20.095	4.4152	−0.009
11	22.677	3.9179	14	2	0	2	22.648	3.9230	−0.030
12				−3	1	1	22.781	3.9004	
13				−3	1	0	22.940	3.8736	
14	22.989	3.8655	17	−2	2	0	22.992	3.8650	0.003
15	23.347	3.8070	5	−2	2	1	23.306	3.8136	−0.041
16	23.710	3.7497	45	0	2	2	23.704	3.7505	−0.006
17				−1	1	3	24.196	3.6753	
18	25.076	3.5483	4	−3	1	2	25.067	3.5495	−0.009
19				2	2	1	25.117	3.5427	
20	25.524	3.4871	4	3	1	1	25.504	3.4898	−0.021
21	25.985	3.4263	11	−2	2	2	25.976	3.4274	−0.009
22				1	1	3	26.784	3.3258	
23				4	0	0	28.171	3.1652	
24	28.314	3.1495	17	1	3	0	28.299	3.1511	−0.015
25				−1	3	1	28.945	3.0823	
26				2	2	2	29.184	3.0576	
27	29.199	3.0560	100	−4	0	2	29.200	3.0559	0.001
28				0	2	3	29.254	3.0504	
29				−3	1	3	29.266	3.0491	
30	29.712	3.0044	11	1	3	1	29.703	3.0053	−0.010
31				3	1	2	29.895	2.9864	
32	30.428	2.9354	7	−2	2	3	30.426	2.9355	−0.002
33				0	0	4	30.475	2.9309	
34				−2	0	4	30.891	2.8924	
35				−1	1	4	31.246	2.8603	
36	31.525	2.8357	11	−1	3	2	31.524	2.8357	−0.001
37	32.914	2.7191	22	1	3	2	32.916	2.7189	0.002
38				−4	2	1	33.276	2.6903	
39	33.748	2.6537	4	4	2	0	33.725	2.6555	−0.024
40	33.969	2.6370	14	1	1	4	34.001	2.6346	0.032
41	34.588	2.5912	16	2	2	3	34.572	2.5923	−0.016
42				−4	2	2	34.604	2.5900	
43				−3	3	1	34.680	2.5845	
44	34.718	2.5818	19	−3	1	4	34.751	2.5794	0.033
45				−3	3	0	34.789	2.5767	
46				4	0	2	34.806	2.5755	
47				3	1	3	35.507	2.5262	
48	35.675	2.5147	5	−1	3	3	35.660	2.5157	−0.015
49				0	2	4	35.706	2.5126	
50				4	2	1	35.892	2.5000	
51				−5	1	1	35.902	2.4993	
52				−2	2	4	36.068	2.4882	
53	36.266	2.4751	4	2	0	4	36.262	2.4753	−0.004
54				−3	3	2	36.278	2.4743	
55				3	3	1	36.592	2.4538	
56	36.641	2.4506	7	5	1	0	36.635	2.4510	−0.006
57				0	4	0	36.804	2.4401	
58	36.830	2.4384	12	−5	1	2	36.840	2.4378	0.010
59	37.290	2.4094	6	−4	0	4	37.324	2.4073	0.033
60	37.517	2.3954	10	1	3	3	37.528	2.3947	0.011
61				−4	2	3	37.545	2.3937	
62	37.621	2.3890	9	0	4	1	37.622	2.3889	0.001
63				−1	1	5	38.696	2.3250	
64				5	1	1	38.957	2.3101	
65	39.326	2.2892	5	−5	1	3	39.346	2.2881	0.020
66				−3	3	3	39.403	2.2849	

Continued

https://doi.org/10.1017/S0885715624000393 Published online by Cambridge University Press

TABLE I. Continued

No.	$2\theta_{obs}$ (°)	d_{obs} (Å)	I/I_o	h	k	l	$2\theta_{cal}$ (°)	d_{cal} (Å)	$\Delta 2\theta$
67				4	2	2	39.533	2.2777	
68	39.549	2.2768	6	2	4	0	39.550	2.2768	0.000
69				−2	4	1	39.743	2.2662	
70	39.878	2.2588	8	3	3	2	39.890	2.2582	0.012
71	39.979	2.2533	7	0	4	2	39.991	2.2527	0.012
72				2	2	4	40.844	2.2076	
73	40.891	2.2052	13	2	4	1	40.891	2.2052	0.000
74				−1	3	4	40.949	2.2022	
75				−3	1	5	41.093	2.1948	
76	41.441	2.1772	5	−2	4	2	41.454	2.1765	0.013
77				1	1	5	41.576	2.1704	
78	41.770	2.1608	11	−4	2	4	41.807	2.1589	0.038
79	41.897	2.1545	9	3	1	4	41.937	2.1526	0.040
80	42.445	2.1280	10	−6	0	2	42.455	2.1275	0.010
81				−2	2	5	42.516	2.1246	
82				5	1	2	42.649	2.1183	
83				0	2	5	42.751	2.1134	
84				6	0	0	42.822	2.1101	
85	43.136	2.0954	13	1	3	4	43.166	2.0941	0.030
86				−5	1	4	43.190	2.0930	
87				2	4	2	43.649	2.0720	
88	43.683	2.0705	16	0	4	3	43.699	2.0697	0.017
89				−3	3	4	43.782	2.0660	
90				4	2	3	44.346	2.0410	
91				3	3	3	44.407	2.0384	
92				−2	4	3	44.537	2.0327	
93				−5	3	1	44.736	2.0242	
94	45.352	1.9981	5	−5	3	0	45.348	1.9982	−0.004
95	45.494	1.9922	4	−5	3	2	45.520	1.9911	0.027
96				−2	0	6	45.700	1.9837	
97				−6	2	1	46.017	1.9707	
98				4	0	4	46.246	1.9615	
99				0	0	6	46.437	1.9539	
100	46.498	1.9515	4	−1	1	6	46.470	1.9526	−0.028
101				−6	2	2	46.530	1.9502	
102				−4	4	1	46.642	1.9458	
103				−6	2	0	46.871	1.9368	
104				−4	4	0	46.982	1.9325	
105				1	5	0	47.065	1.9293	
106				−1	3	5	47.092	1.9282	
107				−4	2	5	47.106	1.9277	
108				5	3	1	47.315	1.9197	
109				5	1	3	47.456	1.9143	
110				−1	5	1	47.486	1.9132	
111	47.623	1.9080	14	2	4	3	47.629	1.9077	0.006
112				−5	3	3	47.648	1.9070	
113				−4	4	2	47.654	1.9068	
114				−6	0	4	47.696	1.9052	
115				2	2	5	47.755	1.9030	
116	47.965	1.8952	7	1	5	1	47.987	1.8943	0.022
117				−3	1	6	48.058	1.8917	
118				−5	1	5	48.120	1.8894	
119				−6	2	3	48.376	1.8800	
120				0	4	4	48.506	1.8753	
121				4	4	1	48.651	1.8700	
122				6	0	2	48.695	1.8684	
123				−2	4	4	48.789	1.8651	

The d-values were calculated using Cu Kα_1 radiation ($\lambda = 1.5405981$ Å).

X'Pert Pro MPD PANalytical diffractometer with a Cu anode ($\lambda = 1.5418$ Å) and a nickel filter. The diffractometer employed the Bragg–Brentano configuration and a high-speed PIXcel solid-state detector for data acquisition with a primary and secondary goniometer radius of 240 mm. A small fraction of the sample was ground and homogenized in an agate mortar and then mounted on a stainless-steel sample holder using the face-fill technique. The diffraction data were collected using a step size of 0.0263° 2θ and a counting time of 97.920 s with a No. of points of 2856. From the powder diffractogram data obtained, crystallographic characterization (indexing and space group determination), whole powder

https://doi.org/10.1017/S0885715624000393 Published online by Cambridge University Press

TABLE II. Atomic coordinates obtained for the compound dichloridodioxido-[(4,7-dimethyl)-1,10-phenanthroline]molybdenum(VI)

Number	Atom	Level	X_{frac}	Y_{frac}	Z_{frac}	B_{iso}	Occupancy
1	C	C1	0.1582	0.8388	1.0192	3.0004	1
2	C	C2	0.1310	0.9666	0.9720	3.0004	1
3	C	C3	0.0622	0.9711	0.8629	3.0004	1
4	C	C4	0.0272	0.8456	0.8095	3.0004	1
5	N	N1	0.0568	0.7225	0.8579	3.0004	1
6	C	C5	0.1199	0.7193	0.9599	3.0004	1
7	H	H1	0.2100	0.8296	1.1023	6.0007	1
8	C	C6	0.1732	1.0955	1.0340	3.0004	1
9	H	H2	0.1409	0.6182	0.9949	6.0007	1
10	C	C13	0.0266	1.0957	0.8042	3.0004	1
11	H	H5	0.0408	1.1787	0.8423	6.0007	1
12	Mo	Mo1	0.0000	0.5272	0.7500	1.0028	1
13	O	O1	0.0441	0.4354	0.8722	3.0004	1
14	Cl	Cl1	0.1650	0.5622	0.6981	3.0004	1
15	H	H10	0.1751	1.0860	1.1251	6.0007	1
16	H	H11	0.1245	1.1846	1.0023	6.0007	1
17	H	H12	0.2538	1.1173	1.0230	6.0007	1

profile decomposition (WPPD), structural elucidation using the simulated annealing method, and refinement using the Rietveld method were then carried out. Finally, the quality of the results obtained was evaluated using the PLATON and DIAMOND programs.

III. RESULTS AND DISCUSSION

The pattern obtained by XRPD was indexed on a monoclinic unit cell with $a = 12.9287$ Å, $b = 9.7604$ Å, $c = 11.9717$ Å, $\beta = 101.688°$, unit-cell volume $V = 1479.376$ Å^3 using TOPAS v.5 (Coelho and Kern, 2004; Bruker AXS GmbH, 2017a, 2017b) (Figure 2, blue line). Analysis of the systematic absences using EXPO2014 (Altomare et al., 2013) suggested the space group C2/c (No. 15) with figures of merit: $M(20) = 20.7$ and $F(30) = 31.3$ (Table I). The refinement of microstructural parameters of polycrystalline material was performed with TOPAS v.5 (Pawley, 1981) fitting using the WPPD procedure employing fundamental parameters (Cheary and Coelho, 1992; Le Bail, 2005; Bruker AXS GmbH, 2017b) (Figure 2, red line). To generate the emission profile, the CuKα5_Berger profile option was selected, and a

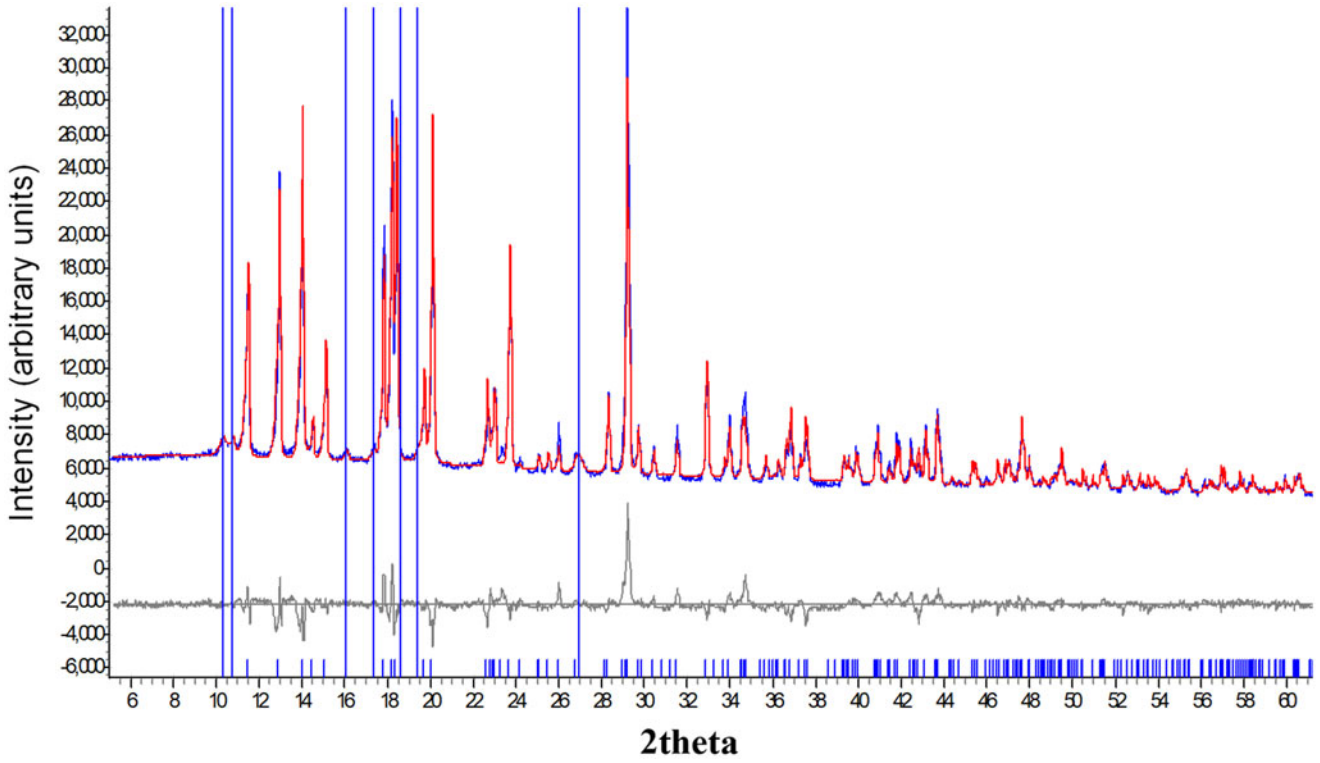

Figure 3. Rietveld refinement result of the dichloridodioxido-[(4,7-dimethyl)-1,10-phenanthroline]molybdenum(VI) (red line). The blue diffractogram corresponds to the experimental profile and the refinement residual is the gray baseline. The perpendicular solid blue lines correspond to the reflections of impurities identified in the material.

https://doi.org/10.1017/S0885715624000393 Published online by Cambridge University Press

TABLE III. Experimental data for dichloridodioxido-[(4,7-dimethyl)-1,10-phenanthroline]molybdenum(VI)

Empirical formula	$C_{14}H_{12}Cl_2MoN_2O_2$
Formula weight	407.106
Crystal system	Monoclinic
Space group	C2/c (No.15)
a/Å	12.9495 (5)
b/Å	9.7752 (4)
c/Å	12.0069 (6)
α/°	90
β/°	101.707 (3)
γ/°	90
Volume/Å^3	1488.27 (11)
Z	4
Z'	0.5
R_{exp}	1.23
R'_{exp}	4.76
R_{wp}	4.65
R'_{wp}	17.96
R_p	3.26
R'_p	19.05
GoF	3.78

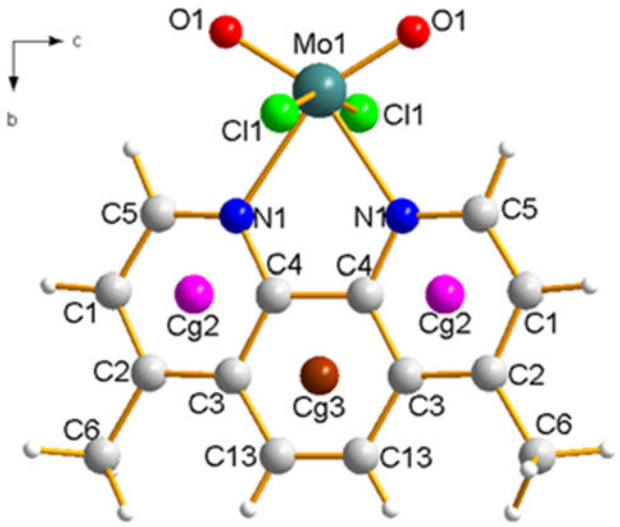

Figure 4. Representation of the molecular structure of the dichloridodioxido-[(4,7-dimethyl)-1,10-phenanthroline]molybdenum(VI) with labeling of atoms and rings. Cg2 and Cg3 refer to the centroids of the aromatic rings.

Chebyshev Polynomial of order 5 was used to fit the background and to obtain the refined unit-cell parameters. Residual values from Pawley fit obtained from the refinement process allowed us to validate the experimental data obtained ($R_{exp} = 1.23$, $R_{wp} = 4.65$, $R_p = 4.65$, $R'_{wp} = 17.96$, $R'_p = 19.05$, and GoF = 3.78). It is important to mention that six weak peaks ($2\theta = 10.342°$, 10.784°, 16.120°, 17.379°, 19.432°, and 27.034°) observed in the experimental diffractogram were excluded from the indexing process and were associated with the presence of remaining impurities of the precursors used in the synthesis which were not possible to eliminate in the purification process, and it was not possible to attribute directly to another specific phase present in the sample.

Once the crystallographic characterization was completed, the structural elucidation was carried out using EXPO2014 program applying the simulated annealing method (Altomare et al., 2009, 2013). The angular range used for the structural determination was 5.0° to 45.0° 2Theta with a

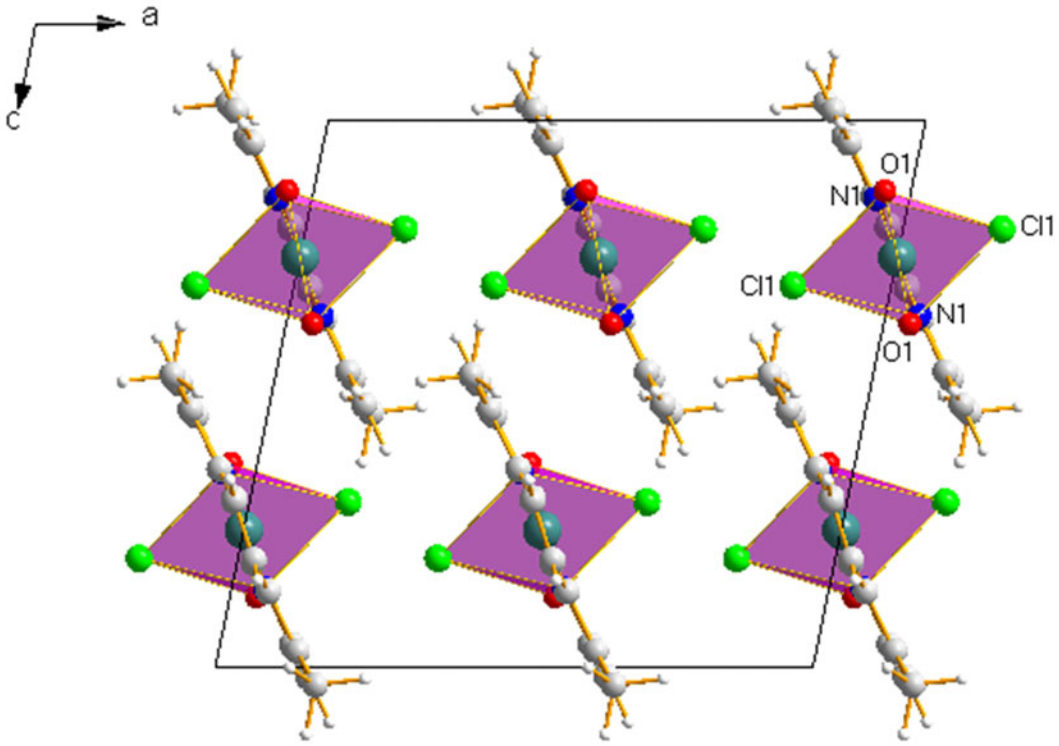

Figure 5. Octahedral coordination of the cis-dioxo-molybdenum (VI) complex coordinated with chlorine and the bidentate nitrogenous ligand 4,7-dimethyl-1,10-phenanthroline.

https://doi.org/10.1017/S0885715624000393 Published online by Cambridge University Press

TABLE IV. Most relevant geometric parameters of the dichloridodioxido-[(4,7-dimethyl)-1,10-phenanthroline]molybdenum(VI)

D–H···A	*D–H* (Å)	*H···A* (Å)	*D–A* (Å)	*D–H···A* (°)	Symmetry operations
(C1–H1···Cl1)[a]	1.09	2.812	3.8139	153	1/2−*x*,3/2−*y*,2−*z*
(C13–H5··· O1)[a]	0.93	2.534	3.4161	158	*x*,1 + *y*,*z*
(C5–H2··· O1)[a]	1.09	2.487	3.0585	112	
CgI···CgJ	*d* (Å)	*α/β/γ* (°)	*Cg*I_Perp/*Cg*J_Perp (Å)		
π–π					
Cg2···Cg2	4.6234	0/41.5/41.5	−3.4632/−3.4632		−*X*,2−*Y*,2−*Z*
Cg2···Cg2	4.5692	0/57.7/57.7	2.4387/24387		1/2−*X*,3/2−*Y*,2−Z
Cg2···Cg3	4.7955	5/42.1/47.0	−3.2680/−3.5591		−*X*,2−*Y*,2−*Z*
Cg2···Cg3	4.7955	5/42.1/47.0	3.2680/−3.5591		*X*,2-*Y*,1/2 + *Z*

Cg2 is the centroid of the ring formed by atoms *C*1 to *C*5 and *N*1. These atoms are reproduced through symmetry to obtain the other aromatic ring, also with the centroid denoted *Cg2* present in the other half of the molecule.
Cg3 is the centroid of the ring formed by the atoms *C*4, *C*3, *C*13, *C*4*, *C*3* *y* *C*13*.
[a]Atoms with atomic positions that are reproduced by symmetry. *D* is the Donor atom; *A* is the acceptor atom.

Chebyshev-type polynomial background noise modeling of order 19. To solve the structure and obtain the best fit between the observed profile and the calculated profile, it was necessary to work with the dynamic occupation model, in turn refining the torsions between the atoms C4:N1:Mo1:O1, C2:C3: C13: H5, and C1:C2:C6:H10. The cost function obtained was 9.719 and the atomic positions of the refined atomic positions are given in Table II.

Finally, the structure obtained was refined using the Rietveld method (least squares) with the TOPAS program, and the function of fundamental parameters was used as a profile modeling function and for peak corrections, the Zero error variable whose value obtained was 0.0646(8). Additionally, the scale factor, cell constants, and possible preferential orientations were refined using the mathematical model of spherical harmonics of order 4. Background was treated using a Chebyshev-type model of order 7, and the microstructural factors corrections using Lorentzian-type Double-Voigt mathematical approximation (Cry size). The signals of the identified impurities are highlighted in blue in Figure 3 and were included in the modeling using the fundamental parameter function refining their position, intensity, and peak width. The final crystallographic parameters obtained are presented in Table III.

Figure 4 shows the molecular structure generated using the Mercury program. The planarity of the phenanthroline rings and the bidentate coordination of the nitrogen atoms with the central metal of molybdenum (VI) were confirmed. The asymmetric unit corresponds to half of the molecule ($Z' = 0.5$) and the other half is reproduced by symmetry, which is why the labels of the atoms are repeated. It is so the chlorine, nitrogen, oxygen, and molybdenum atoms form a distorted

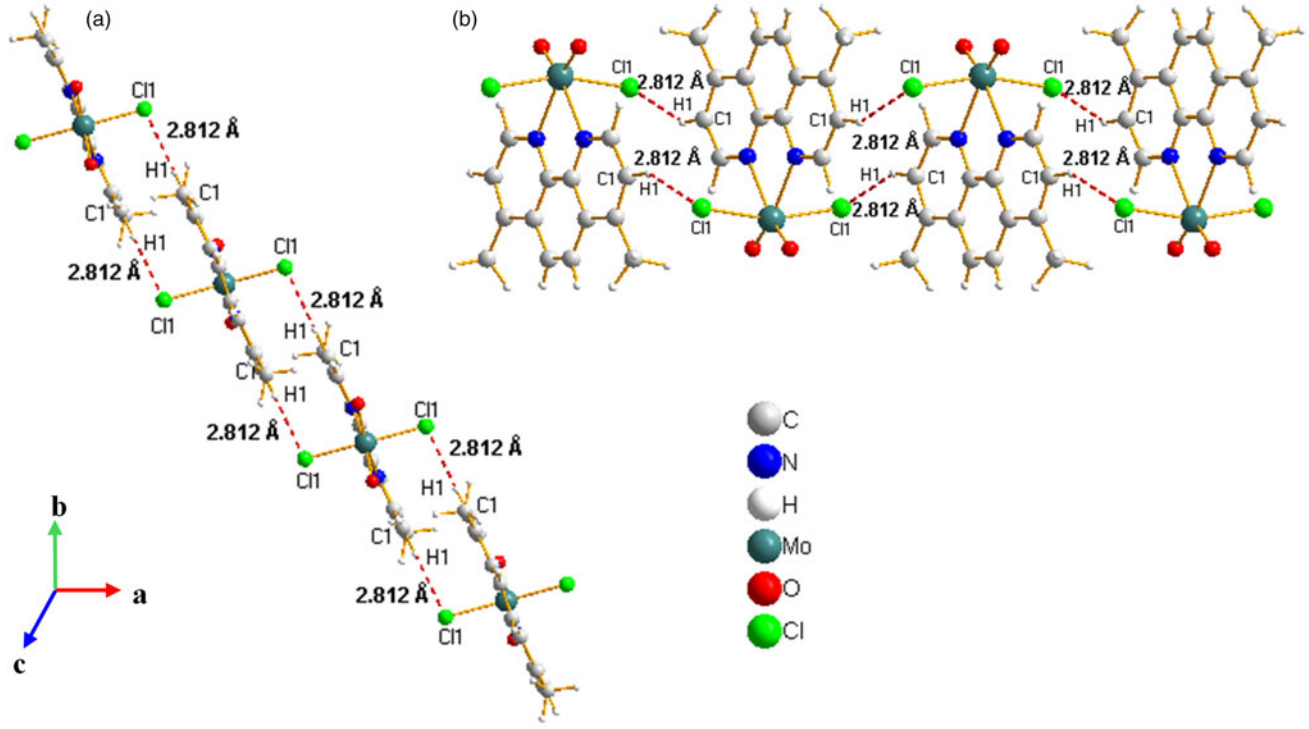

Figure 6. Representation of the intermolecular interactions of the C1–H1···Cl1 atoms in the crystalline packing of dichloridodioxido-[(4,7-dimethyl)-1,10-phenanthroline]molybdenum(VI).

https://doi.org/10.1017/S0885715624000393 Published online by Cambridge University Press

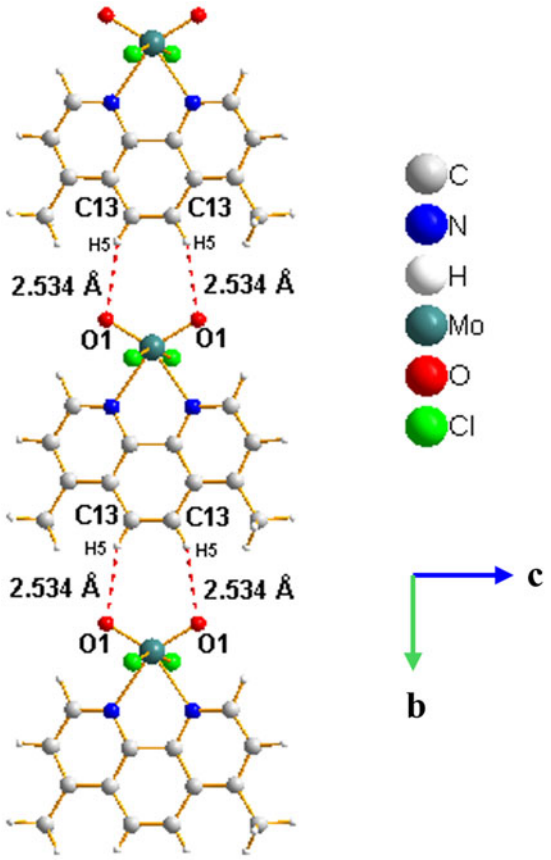

Figure 7. Representation of the intermolecular interactions of the C13–H5···O1 atoms in the crystalline packing of dichloridodioxido-[(4,7-dimethyl)-1,10-phenanthroline]molybdenum(VI).

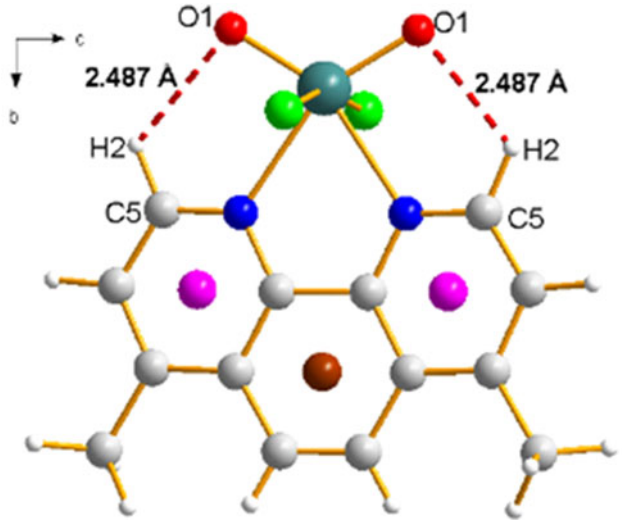

Figure 8. Representation of the intramolecular interactions between C5–H2···O1 atoms in the crystalline packing of dichloridodioxido-[(4,7-dimethyl)-1,10-phenanthroline]molybdenum(VI).

octahedral coordination geometry with a volume of 12.307 Å^3 and a quadratic elongation of 1.063 (Figure 5).

Previous research has established that the chlorine atoms are in *-trans-* position, while the oxygen and nitrogen atoms of the phenanthroline ligand are in the *cis*-configuration, generating greater stability in the molecule as a product of their respective electronic contributions. This preferential configuration (-cis-oxo, trans-Halogen, cis-N–N) has been previously studied by both experimental and theoretical measurements in bioinspired complexes of molybdenum or tungsten using ligands such as the chlorine, bromine fluorine, and bidentate ligands such as bipyridines and Schiff bases (Pietsch and Hall, 1996; Barea et al., 1998; Hofmann, 2006; Agustin et al., 2009; Roy et al., 2021).

A. Intermolecular hydrogen bonds

The geometry of the different intermolecular interactions and the π–π interactions between the centroid rings *CgI* and *CgJ* (*I* take the values of 2 and *J* take the values of 2 or 3) were determined through the PLATON program (Spek, 2003, 2015, 2020), where it was specified that *Cg2* and *Cg3* are the centroids of rings 2 and 3 as described in Figure 4. The value of *d* refers to the distance between the centroids *CgI*···*CgJ*, α corresponds to the dihedral angle between planes

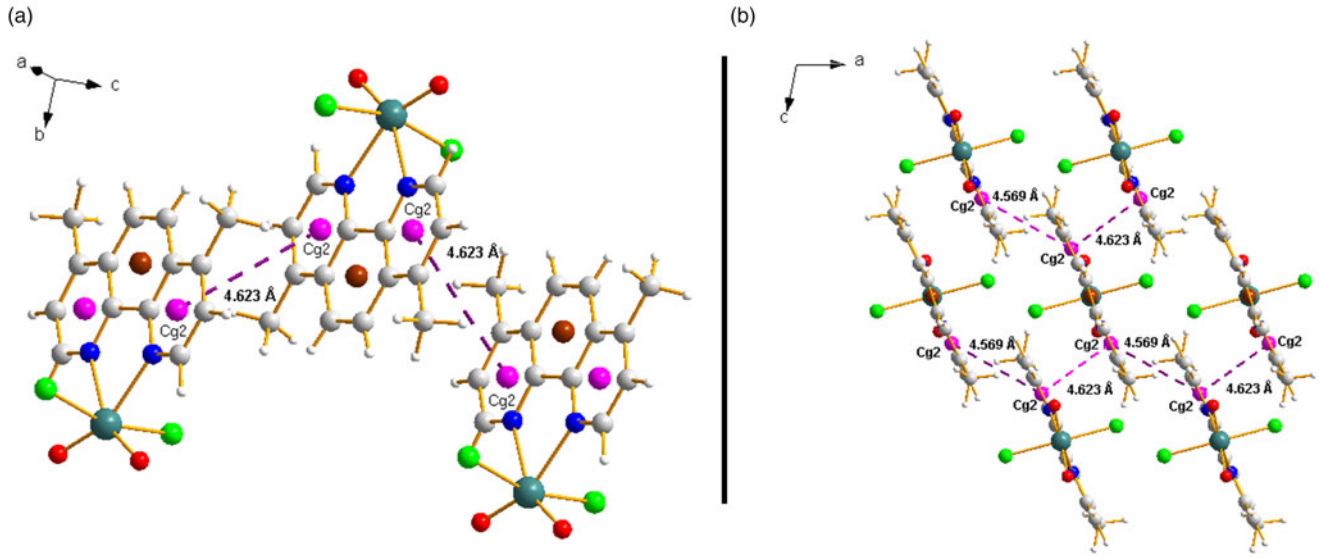

Figure 9. π–π interactions of the *Cg2* centroids between neighborhood molecules (a) along the axes *a* (b) along the axes *c*.

https://doi.org/10.1017/S0885715624000393 Published online by Cambridge University Press

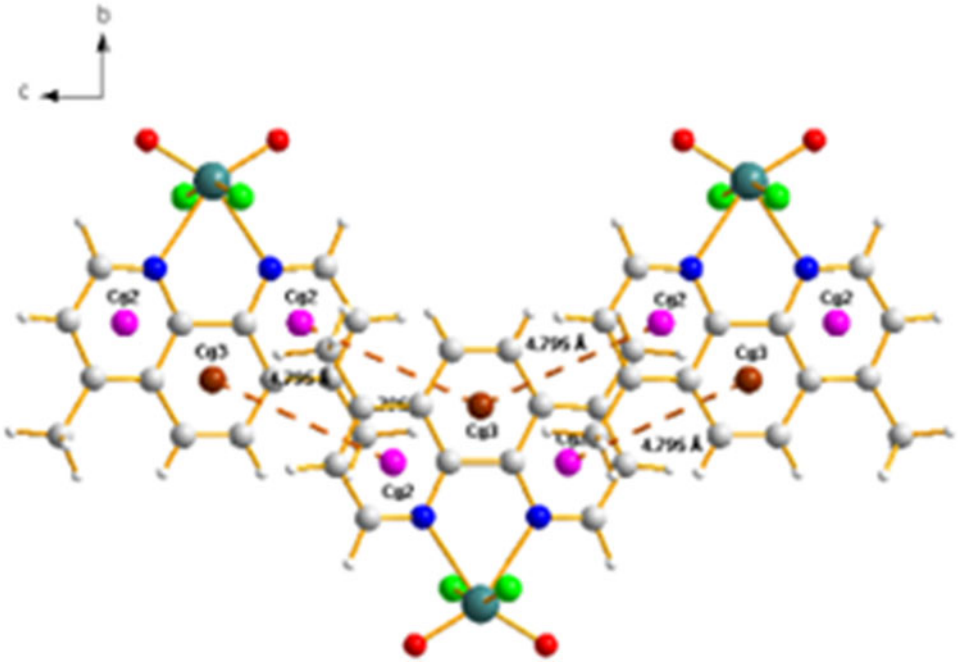

Figure 10. π–π interactions between the centroid *Cg2* and the centroid *Cg3* along the axes *a*.

I and *J*, β is the angle between the vector *Cg(I)* → *Cg(J)* and the normal to plane *I*, γ is the angle between the vector *Cg(I)* → *Cg(J)* and the normal to the plane *J*, *CgI*_Perp is the perpendicular distance of the centroid *CgI* on the ring *J*, and *CgJ*_Perp is the perpendicular distance of the centroid *CgJ* on the ring *I*. Table IV summarizes the most relevant geometric parameters generated by the variety of interactions between hydrogen bond donor (D) and acceptor (A) atoms.

The structural elucidation process revealed the presence of four intermolecular hydrogen bonds. The C1–H1···Cl1

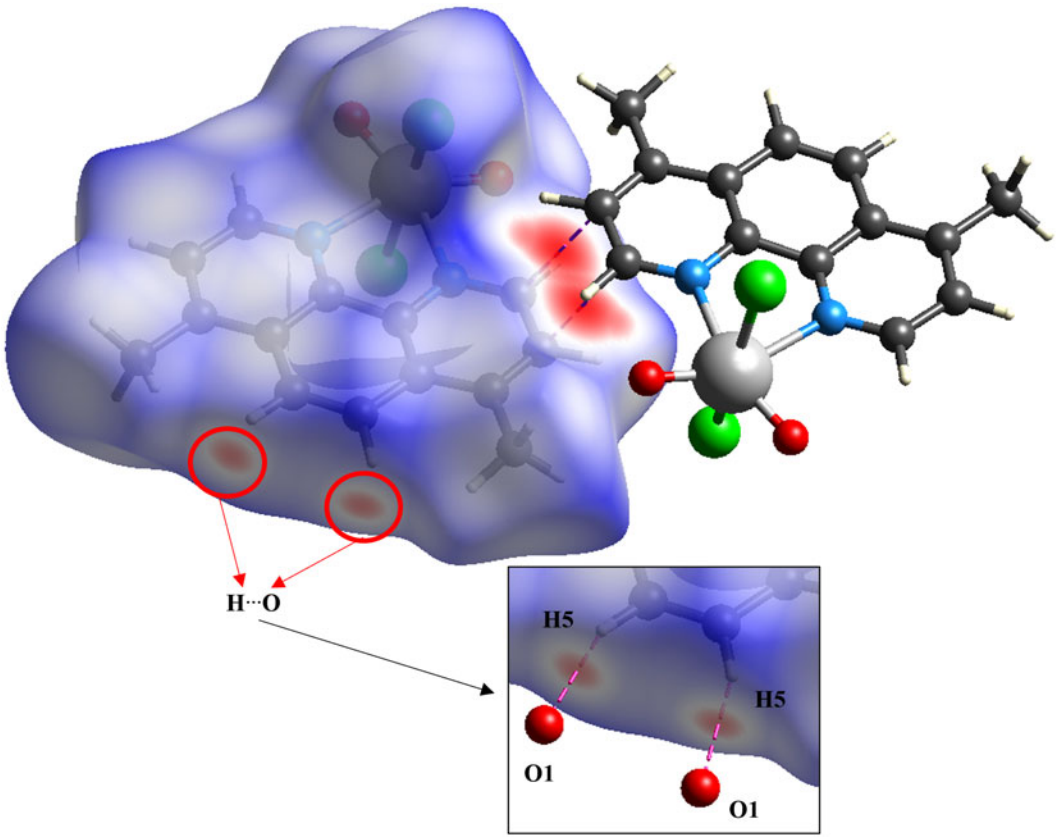

Figure 11. Analysis of the Hirshfeld surface (d_{norm} surface) of the dichloridodioxido-[(4,7-dimethyl)-1,10-phenanthroline]molybdenum(VI). The boxes show the atoms of the surrounding molecule with which the interaction is generated.

https://doi.org/10.1017/S0885715624000393 Published online by Cambridge University Press

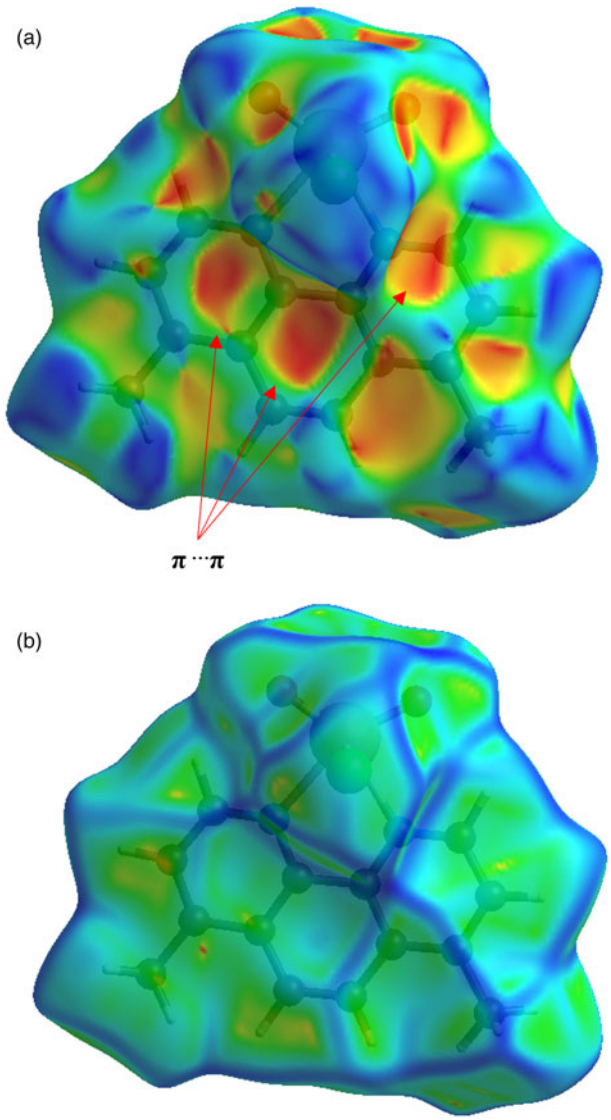

Figure 12. Hirshfeld surface analysis of the structure of the dioxo-molybdenum (VI) complex, (a) shape index and (b) curvature.

(2 interactions throughout the molecule) which in a projection on the *c* axis, form zigzag chains along the *a* axis [Figure 6(a)], and in the projection along the *b* axis are organized forming chains diagonally along the *a* and *c* axes [Figure 6(b)]. Furthermore, the other two intermolecular hydrogen atoms are present in the C13–H5···O1 bonds form linear chains along the *b* axis whose distance between the hydrogen atom and the oxygen atom corresponds to 2.534 Å (Figure 7).

Additionally, the analysis of the structure also indicates the existence of two intramolecular hydrogen bonds (C5–H2···O1) that help in the stability of the bonds of the octahedral system formed by the central molybdenum atom. In Figure 8, these interactions are observed in a projection along the *a* axis.

B. π–π interactions

In addition to hydrogen bond interactions, connectivity between the molecules was also determined through π–π interactions. Figure 9 shows the π–π interactions generated between the centroids Cg2···Cg2, at distances of 4.623 and 4.569 Å. These interactions are related to the symmetry operations $-X$, $2-Y$, $2-Z$, and $1/2-X$, $3/2-Y$, $2-Z$ (Table IV), evidencing the formation of chains diagonally along the axes *a* and *c*.

The π–π interaction obtained at a longer distance (d = 4.795 Å) was determined between the centroid of ring 2 (*Cg2*) and the centroid of ring 3 (*Cg3*) of its neighboring molecule. This π–π interaction is associated with the X, $2-Y$, $2-Z$; X, $2-Y$, $1/2+Z$; X, $2-Y$, $-1/2+Z$ symmetry operation. and is presented in a projection along the *a* axis in Figure 10.

C. Hirshfeld surface analysis

The calculated Hirshfeld surface mapped over the normalized contact distance d_{norm} and the associated two-dimensional fingerprint plots of the dioxo-molybdenum complex (VI) were calculated using CrystalExplorer21 (Spackman et al., 2021). Hirshfeld surfaces mapped on d_{norm} use the function of normalized distances from a given point to the closest atom inside (d_i) and outside (d_e) the surface (Spackman and Jayatilaka, 2009). The blue, white, and red color conventions used for Hirshfeld surfaces show long, van der Waals, and short interatomic contacts, respectively. Figure 11 shows the short-range interactions between the atoms H···O (H5···O1) and C···C (C1···C5 y C5···C1) with a distance between atoms of 2.534 and 2.890 Å, respectively.

The shape index and the curvature surfaces provide a greater chemical understanding of the packing of the complex. Figure 12(a) presents the shape index obtained, where the interactions of the atoms present in the aromatic rings (π···π interactions) of the complex are highlighted. The region, atom, or zone that acts as a donor corresponds to blue color and the acceptor is represented with a red color. It is important to mention that surface shape is only a qualitative analysis of the donor–acceptor interactions. Additionally, in Figure 12(b), the curvature surface is presented from which it is possible to define that there are no flat areas in the structure, which is an indication of the absence of stacking of one structure on top of another in the packing.

Finally, Figure 13 presents the fingerprint plots of the contributions corresponding to the most important interactions on the surface of the dichloridodioxido-[(4,7-dimethyl)-1,10-phenanthroline]molybdenum(VI) complex structure. In the crystalline packing, the greatest contributions were obtained by the interactions H···Cl/Cl···H, H···C/C···H, H···O/O···H, and H ···H whose percentages are 30.2%, 23.4%, 20.3%, and 16.5%, respectively. Additionally, the C···Cl/Cl···C, C···C, N···H/H···N contacts contribute in a percentage of 3.3%, 2.3%, and 2.2%, respectively. Some other interactions with contributions to a lesser degree reached a percentage of 1.8%.

IV. DEPOSITED DATA

The CIF (Chemical Information File) of the compound was deposited with ICDD. The data can be requested from the Managing Editor at pdj@icdd.com.

https://doi.org/10.1017/S0885715624000393 Published online by Cambridge University Press

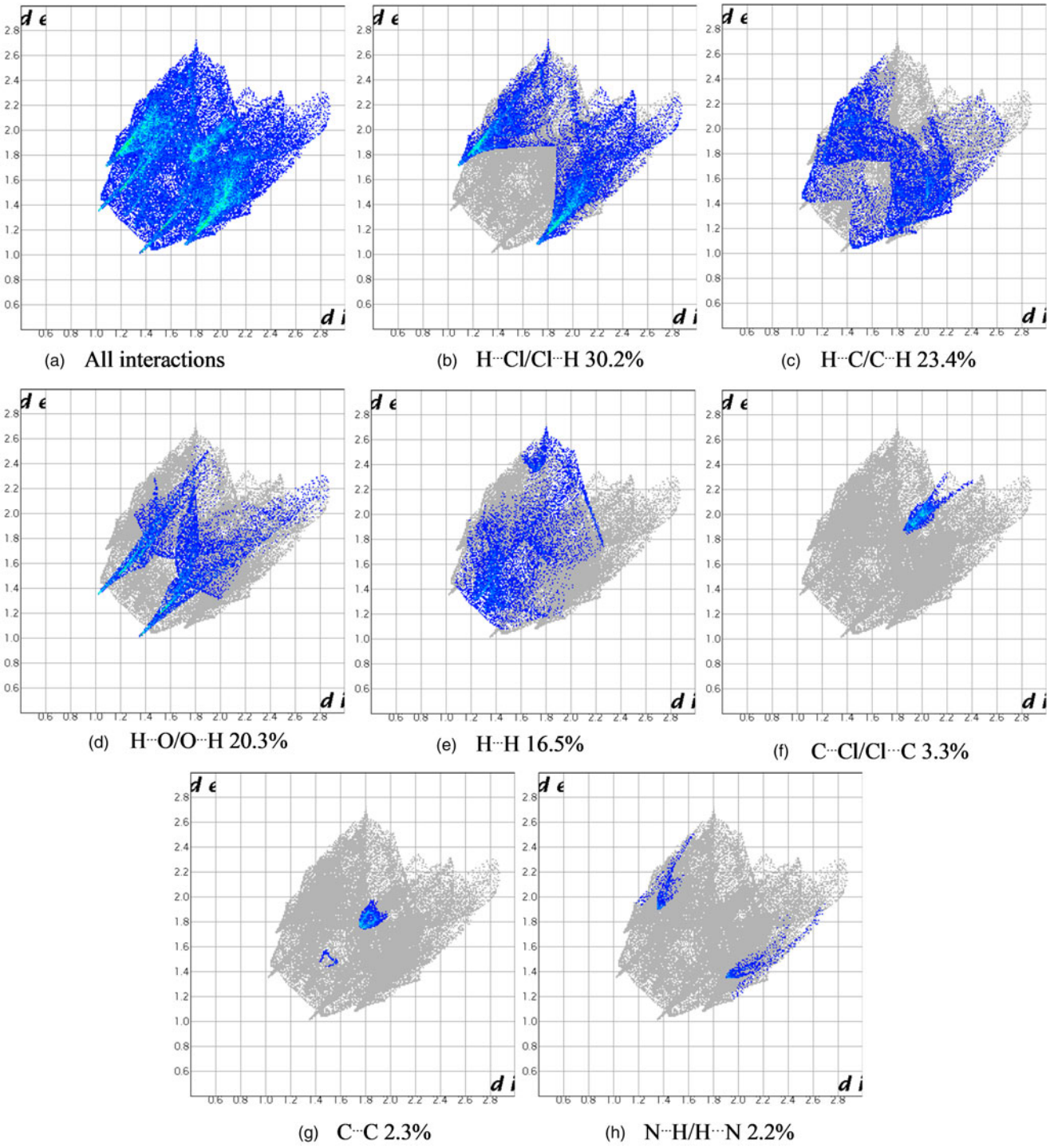

Figure 13. Fingerprints and their contributions in percentage for the most relevant interactions on the surface of the dichloridodioxido-[(4,7-dimethyl)-1,10-phenanthroline]molybdenum(VI) complex.

ACKNOWLEDGEMENTS

This work was financially supported by the Facultad de Ciencias at Universidad Nacional de Colombia by the internal Projects code 57674. NJC appreciates the collaboration from the X-Ray Diffraction laboratory for the support with the analysis of the samples and Geology Department for the access to the EVA and TOPAS programs.

CONFLICTS OF INTEREST

The authors have no conflicts of interest to declare.

REFERENCES

Agustin, D., C. Bibal, B. Neveux, J. C. Daran, and R. Poli. 2009. "Structural Characterization and Theoretical Calculations of Cis-dioxo(Nsalicylidene-2-Aminophenolato)(Ethanol)Molybdenum(VI) Complexes MoO2(SAP)(EtOH) (SAP = N-Salicylidene-2 Aminophenolato)." *Zeitschrift Fur Anorganische Und Allgemeine Chemie* 635 (13–14): 2120–5. doi:10.1002/zaac.200900185.

Altomare, A., M. Camalli, C. Cuocci, C. Giacovazzo, A. Moliterni, and R. Rizzi. 2009. "EXPO2009: Structure Solution by Powder Data in Direct and Reciprocal Space." *Journal of Applied Crystallography* 42 (6): 1197–202. doi:10.1107/S0021889809042915.

Altomare, A., C. Cuocci, C. Giacovazzo, A. Moliterni, R. Rizzi, N. Corriero, and A. Falcicchio. 2013. "EXPO2013: A Kit of Tools for Phasing Crystal

https://doi.org/10.1017/S0885715624000393 Published online by Cambridge University Press

Structures From Powder Data." *Journal of Applied Crystallography* 46 (4): 1231–5. doi:10.1107/S0021889813013113.

Anastas, P. T., and M. M. Kirchhoff. 2002. "Origins, Current Status, and Future Challenges of Green Chemistry." *Accounts of Chemical Research* 35 (9): 686–694. doi:10.1021/ar010065m.

Arzoumanian, H. 1998. "Molybdenum-oxo Chemistry in Various Aspects of Oxygen Atom Transfer Processes." *Coordination Chemistry Reviews* 178–180 (PART 1): 191–202. doi:10.1016/s0010-8545(98)00056-3.

Arzoumanian, H., R. Lopez, and G. Agrifoglio. 1994. "Synthesis and X-ray Characterization of Tetraphenylphosphonium Tetrathiocyanatodioxomolybdate(VI): A Remarkable Oxo Transfer Agent." *Inorganic Chemistry* 33 (14): 3177–3179. doi:10.1021/ic00092a026.

Arzoumanian, H., R. Bakhtchadjian, G. Agrifoglio, R. Atencio, and A. Briceño. 2006. "Synthesis and Characterization of Halo, Cyanato, Thiocyanato and Selenocyanato Molybdenum(VI) Dioxo and Dioxo-μ-oxo Complexes." *Transition Metal Chemistry* 31 (5): 681–689. doi:10.1007/S11243-006-0049-6/METRICS.

Bakhtchadjian, R., S. Tsarukyan, J. Barrault, F. O. Martinez, L. Tavadyan, and N. J. Castellanos. 2011. "Application of a Dioxo-Molybdenum(VI) Complex Anchored on TiO_2 for the Photochemical Oxidative Decomposition of 1-chloro-4-ethylbenzene Under O_2." *Transition Metal Chemistry* 36 (8): 897–900. doi:10.1007/s11243-011-9547-2.

Barea, G., A. Lledos, F. Maseras, and Y. Jean. 1998. "Cis,trans,cis or All-cis Geometry in d0 Octahedral Dioxo Complexes. An IMOMM Study of the Role of Steric Effects." *Inorganic Chemistry* 37 (13): 3321–5. doi:10.1021/ic971226e.

Bencini, A., and V. Lippolis. 2010. "1,10-Phenanthroline: A Versatile Building Block for the Construction of Ligands for Various Purposes." *Coordination Chemistry Reviews* 254 (17–18): 2096–180. doi:10.1016/J.CCR.2010.04.008.

Bouzari, N., A. Bezaatpour, B. Babaei, M. Amiri, R. Boukherroub, and S. Szunerits. 2021. "Modification of $MnFe_2O_4$ Surface by Mo (VI) Pyridylimine Complex as an Efficient Nanocatalyst for (ep)oxidation of Alkenes and Sulfides." *Journal of Molecular Liquids* 330: 115690. doi:10.1016/J.MOLLIQ.2021.115690.

Bruker AXS GmbH. 2017a. DIFFRACT.SUITE, User Manual: TOPAS, Technical Reference.

Bruker AXS GmbH. 2017b. Whole Powder Pattern Decomposition. In *TOPAS Tutorial, User Manual* (pp. 34–38). Bruker.

Camargo, H. A., J. A. Henao, and N. J. Castellanos. 2016. "Synthesis and X-ray Diffraction Data for Dibromo-dioxo-(1,10-phenanthroline-N,N′)-Molybdenum(VI) ($C_{12}H_8N_2MoBr_2O_2$)." *Powder Diffraction* 31 (1): 66–70. doi:10.1017/S0885715615000949.

Castellanos, N. J., F. Martínez, E. A. Páez-Mozo, F. Ziarelli, and H. Arzoumanian. 2012. "Bis(3,5-Dimethylpyrazol-1-yl)Acetate Bound to Titania and Complexed to Molybdenum Dioxido as a Bidentate N, N′-Ligand. Direct Comparison with a Bipyridyl Analog in a Photocatalytic Arylalkane Oxidation by O_2." *Transition Metal Chemistry* 37 (7): 629–37. doi:10.1007/s11243-012-9631-2.

Castellanos, N. J., F. Martínez, F. Lynen, S. Biswas, P. Van Der Voort, and H. Arzoumanian. 2013. "Dioxygen Activation in Photooxidation of Diphenylmethane by a Dioxomolybdenum(VI) Complex Anchored Covalently onto Mesoporous Titania." *Transition Metal Chemistry* 38 (2): 119–127. doi:10.1007/s11243-012-9668-2.

Castellanos, N. J., H. Martínez Q, F. Martínez O, K. Leus, and P. Van Der Voort. 2021. "Photo-Epoxidation of (α, β)-Pinene with Molecular O_2 Catalyzed by a Dioxo-Molybdenum (VI)-Based Metal–Organic Framework." *Research on Chemical Intermediates* 47 (10): 4227–44. doi:10.1007/s11164-021-04518-3.

Cheary, R. W., and A. Coelho. 1992. "Fundamental Parameters Approach to X-Ray Line-Profile Fitting." *Journal of Applied Crystallography* 25 (pt 2): 109–21. doi:10.1107/S0021889891010804.

Coelho, A., and A. Kern. 2004. "Discussion of the Indexing Algorithms Within TOPAS." *Commision of Powder Diffraction* 32: 43.

Dupé, A., M. E. Judmaier, F. Belaj, K. Zangger, and N. C. Mösch-Zanetti. 2015. "Activation of Molecular Oxygen by a Molybdenum Complex for Catalytic Oxidation." *Dalton Transactions* 44 (47): 20514–22. doi:10.1039/c5dt02931g.

Heinze, K. 2015. "Bioinspired Functional Analogs of the Active Site of Molybdenum Enzymes: Intermediates and Mechanisms." *Coordination Chemistry Reviews* 300: 121–41. doi:10.1016/j.ccr.2015.04.010.

Hermans, I., E. S. Spier, U. Neuenschwander, N. Turrà, and A. Baiker. 2009. "Selective Oxidation Catalysis: Opportunities and Challenges." *Topics in Catalysis* 52 (9): 1162–74. doi:10.1007/s11244-009-9268-3.

Hille, R. 2002. "Molybdenum and Tungsten in Biology." *Trends in Biochemical Sciences* 27 (7): 360–7. doi:10.1016/S0968-0004(02)02107-2.

Hille, R., T. Nishino, and F. Bittner. 2011. "Molybdenum Enzymes in Higher Organisms." *Coordination Chemistry Reviews* 255 (9–10): 1179–205. doi:10.1016/j.ccr.2010.11.034.

Hofmann, M. 2006. "What is the Best Theoretical Method to Study Molybdenum Dithiolene Complexes?" *Journal of Molecular Structure: THEOCHEM* 773 (1–3): 59–70. doi:10.1016/J.THEOCHEM.2006.06.036.

Hone, C. A., and C. O. Kappe. 2019. "The Use of Molecular Oxygen for Liquid Phase Aerobic Oxidations in Continuous Flow." *Topics in Current Chemistry* 377 (1): 1–44. doi:10.1007/s41061-018-0226-z.

Julião, D., A. C. Gomes, L. Cunha-Silva, M. Pillinger, I. S. Gonçalves, and S. S. Balula. 2022. "Dichloro and Dimethyl Dioxomolybdenum(VI)-Bipyridine Complexes as Catalysts for Oxidative Desulfurization of Dibenzothiophene Derivatives Under Extractive Conditions." *Journal of Organometallic Chemistry* 967: 122336. doi:10.1016/j.jorganchem.2022.122336.

Kargar, H., M. Fallah-Mehrjardi, R. Behjatmanesh-Ardakani, K. S. Munawar, M. Ashfaq, and M. N. Tahir. 2021. "Selective Oxidation of Benzyl Alcohols to Benzaldehydes Catalyzed by Dioxomolybdenum Schiff Base Complex: Synthesis, Spectral Characterization, Crystal Structure, Theoretical and Computational Studies." *Transition Metal Chemistry* 46 (6): 437–55. doi:10.1007/s11243-021-00460-w.

Kühn, F. E., A. M. Santos, and M. Abrantes. 2006. "Mononuclear Organomolybdenum(VI) Dioxo Complexes: Synthesis, Reactivity, and Catalytic Applications." *Chemical Reviews* 106 (6): 2455–75. doi:10.1021/cr040703p.

Le Bail, A. 2005. "Whole Powder Pattern Decomposition Methods and Applications: A Retrospection." *Powder Diffraction* 20 (4): 316–26. doi:10.1154/1.2135315.

Martinez Q, H., Á. A. Amaya, E. A. Paez-Mozo, F. Martinez O, and S. Valange. 2020. "Photo-Assisted O-Atom Transfer to Monoterpenes With Molecular Oxygen and a dioxoMo(VI) Complex Immobilized on TiO_2 Nanotubes." *Catalysis Today* 375, 441–457. doi:10.1016/j.cattod.2020.07.053.

Martínez, H., M. F. Cáceres, F. Martínez, E. A. Páez-Mozo, S. Valange, N. J. Castellanos, D. Molina, J. Barrault, and H. Arzoumanian. 2016. "Photo-Epoxidation of Cyclohexene, Cyclooctene and 1-Octene With Molecular Oxygen Catalyzed by Dichloro Dioxo-(4,4′-Dicarboxylato-2,2′-Bipyridine) Molybdenum(VI)Grafted on Mesoporous TiO_2." *Journal of Molecular Catalysis A: Chemical* 423: 248–55. doi:10.1016/j.molcata.2016.07.006.

Nunes, M. S., A. C. Gomes, P. Neves, R. F. Mendes, F. A. Almeida Paz, A. D. Lopes, M. Pillinger, I. S. Gonçalves, and A. A. Valente. 2023. "Molybdenum(VI) Complexes With Ligands Derived from 5-(2-pyridyl)-2H-Tetrazole as Catalysts for the Epoxidation of Olefins." *Catalysis Today* 423: 114273. doi:10.1016/J.CATTOD.2023.114273.

Pawley, G. S. 1981. "Unit-Cell Refinement from Powder Diffraction Scans." *Journal of Applied Crystallography* 14 (6): 357–61. doi:10.1107/s0021889881009618.

Pietsch, M. A., and M. B. Hall. 1996. "Theoretical Studies on Models for the Oxo-Transfer Reaction of Dioxomolybdenum Enzymes." *Inorganic Chemistry* 35 (5): 1273–8. doi:10.1021/ic951044p.

Qin, Y., B. Wang, J. Li, X. Wu, and L. Chen. 2019. "Cobalt Imine–Pyridine–Carbonyl Complex Functionalized Metal–Organic Frameworks as Catalysts for Alkene Epoxidation." *Transition Metal Chemistry* 44 (7): 595–602. doi:10.1007/s11243-019-00319-1.

Roduner, E., W. Kaim, B. Sarkar, V. B. Urlacher, J. Pleiss, R. Gläser, W. D. Einicke, G. A. Sprenger, U. Beifuß, E. Klemm, C. Liebner, H. Hieronymus, S. F. Hsu, B. Plietker, and S. Laschat. 2013. "Selective Catalytic Oxidation of C-H Bonds with Molecular Oxygen." *Chemcatchem* 5 (1): 82–112. doi:10.1002/cctc.201200266.

Roy, M., D. Biswal, N. R. Pramanik, M. G. B. Drew, S. Paul, P. Kachhap, C. Haldar, and S. Chakrabarti. 2021. "Structural Elucidation, DFT Calculations and Catalytic Activity of Dioxomolybdenum(VI) Complexes With N–N Donor Ligand: Role of Halogen Atom Coordinated to the Molybdenum Centre." *Polyhedron* 200: 115144. doi:10.1016/j.poly.2021.115144.

Shen, Y., and B. Patrick Sullivan. 1995. "A Versatile Preparative Route to 5-Substituted-1,10-Phenanthroline Ligands via 1,10-Phenanthroline 5,6-Epoxide." *Inorganic Chemistry* 34 (25): 6235–6. doi:10.1021/ic00129a003.

Spackman, M. A., and D. Jayatilaka. 2009. "Hirshfeld Surface Analysis." *Crystengcomm* 11 (1): 19–32. doi:10.1039/b818330a.

Spackman, P. R., M. J. Turner, J. J. McKinnon, S. K. Wolff, D. J. Grimwood, D. Jayatilaka, and M. A. Spackman. 2021. "Crystalexplorer: A Program for Hirshfeld Surface Analysis, Visualization and Quantitative Analysis of Molecular Crystals." *Journal of Applied Crystallography* 54: 1006–11. doi:10.1107/S1600576721002910.

Spek, A. L. 2003. "Single-Crystal Structure Validation with the Program PLATON." *Journal of Applied Crystallography* 36 (1): 7–13. doi:10.1107/S0021889802022112.

Spek, A. L. 2015. "PLATON SQUEEZE: A Tool for the Calculation of the Disordered Solvent Contribution to the Calculated Structure Factors." *Acta Crystallographica Section C: Structural Chemistry* 71 (1): 9–18. doi:10.1107/S2053229614024929.

Spek, A. L. 2020. "CheckCIF Validation ALERTS: What They Mean and How to Respond." *Acta Crystallographica Section E: Crystallographic Communications* 76: 1–11. doi:10.1107/S2056989019016244.

Zwettler, N., M. A. Ehweiner, J. A. Schachner, A. Dupé, F. Belaj, and N. C. Mösch-Zanetti. 2019. "Dioxygen Activation With Molybdenum Complexes Bearing Amide-Functionalized Iminophenolate Ligands." *Molecules* 24 (9), 1814. doi:10.3390/molecules24091814.